

Phonons in ultrathin oxide films – 2D to 3D transition in FeO on Pt(111)

N. Spiridis,¹ M. Zając,^{2,3,a} P. Piekarz,⁴ A.I. Chumakov,² K. Freindl,¹ J. Goniakowski,^{5,6} A. Koziół-Rachwał,³ K. Parliński,⁴ M. Ślęzak,³ T. Ślęzak,³ U. Wdowik,⁷ D. Wilgocka-Ślęzak,¹ J. Korecki,^{1,3,*}

¹*Jerzy Haber Institute of Catalysis and Surface Chemistry, Polish Academy of Sciences, ul. Niezapominajek 8, 30-239 Kraków, Poland.*

²*European Synchrotron Radiation Facility (ESRF), P.O. Box 220, F-38043 Grenoble, France*

³*Faculty of Physics and Applied Computer Science, AGH University of Science and Technology, al. Mickiewicza 30, 30-059 Kraków, Poland*

⁴*Institute of Nuclear Physics, Polish Academy of Sciences, ul. Radzikowskiego 152, 31342 Kraków, Poland*

⁵*CNRS, Institut des Nanosciences de Paris, UMR 7588, 4 place Jussieu, 75005 Paris, France*

⁶*UPMC Univ Paris 06, INSP, UMR 7588, 4 place Jussieu, 75252 Paris CEDEX, France*

⁷*Institute of Technology, Pedagogical University, ul. Podchorążych 2, PL-30084 Kraków, Poland*

*korecki@agh.edu.pl

^a present address: National Synchrotron Radiation Centre SOLARIS at Jagiellonian University, ul. Gołębia 24, 31-007 Kraków, Poland

Abstract

The structural and magnetic properties of ultrathin FeO(111) films on Pt(111) with thicknesses from 1 to 16 monolayers (ML) were studied using the nuclear inelastic scattering (NIS) of synchrotron radiation. Distinct evolution of vibrational characteristics with thickness that is revealed in the phonon density of states (PDOS) witnesses a textbook transition from 2D to 3D lattice dynamics. For the thinnest films of 1 and 2 ML, the low energy part of the PDOS followed a linear $\propto E$ dependence in energy that is characteristic for 2-dimensional systems. This dependence gradually transforms with thickness to the bulk $\propto E^2$ relation. Density functional theory phonon calculations perfectly reproduced the measured 1 ML PDOS within a simple model of a pseudomorphic FeO/Pt(111) interface. In this model, a weak coupling to the Pt(111) substrates results in a quasi-free-standing FeO film behavior. The evolution of the vibrational properties with an increasing thickness is closely related to a transient long range magnetic order and stabilization of an unusual structural phase.

Dimensionality has the major impact on the basic properties of the condensed matter. In low-dimensional systems, the confinement of electrons and phonons changes their dispersion relations and density of states, which is reflected in modifications of electrical, magnetic, thermal and optical properties when going from the 3-dimensional (3D) bulk to a 2-dimensional (2D) monolayer.¹ The effect of the reduced dimensionality is relatively simple to observe for the electronic system thanks to the short characteristic length and large energy level splitting. Furthermore, from the electronic point of view, also supported monolayers can be considered as quasi-free-standing if their electronic states do not overlap with those of the substrate. Conversely, due to the collective character of lattice vibrations, truly 2D phononic systems are limited to monolayer membranes, like graphene¹ or similar quasi two-dimensional systems.² Primary information on the crystal structure that is contained in the vibrational properties put the challenge to directly measure the phonon spectra in low dimensional systems. Phonons determine elastic and thermodynamic properties and mediate many coupling phenomena. Phonons also promote phase transitions that are predictable from dispersion relations.³

Important class of low-dimensional materials are oxides. Ultrathin epitaxial oxide films are of recent interest for basic and applied research as model catalysts, sensors, in microelectronics and spintronics, and other applications.⁴ The extent to which the properties of films comprising a few atomic layers down to the monolayer resemble those of their bulk counterparts is an increasingly important question. The problem is complex from structural and electronic points of view, and first-principle calculations show a specific crystal⁵ and electronic structure⁶ of oxide surfaces and metal-supported oxide monolayers.⁷ Metastable oxide structures can be stabilized in epitaxial ultrathin films as a result of the intricate interplay of different film and substrate parameters.⁸ Especially, polarity compensation may be the driving factor of artificial structure stabilization, however the stability is often limited to a couple of monolayers.^{9,10,11} In one of the most extensively studied polar oxide-film systems, i.e. for FeO(111) films on Pt(111),¹² it was possible to extend the structural stability beyond the monolayer range.¹³ This gave us opportunity to systematic study the evolution of the vibrational properties characteristic for a 2D to 3D-transition which is the subject of the present paper.

We have measured the partial iron phonon density of states (PDOS) as a function of FeO film thickness from a single to over a dozen monolayers using the nuclear inelastic scattering

(NIS) of synchrotron radiation,^{14,15} and we showed that the PDOS is distinctly different from bulk FeO (wüstite) over the thickness range. Particularly, the monolayer PDOS is characterized by a sharp feature at an energy of $E=24$ meV, which is well-explained within a structural model used in density functional theory (DFT) phonon calculations. Furthermore, instead of the Debye-like- $\propto E^2$ behavior, PDOS scales linearly with energy in the monolayer range that represents truly 2-dimensional behavior. A gradual transition toward the 3D characteristics with thickness is accompanied by magnetic anomalies that are distinctly reflected in the phonon spectra.

Bulk FeO has an NaCl-type wüstite structure, and the (111)-oriented FeO epitaxial films are considered to represent the fcc stacking of alternating hexagonal iron and oxygen planes.¹² A considerable (10%) lattice mismatch between Pt(111) and FeO(111) (in plane spacing of surface atoms $a_{\text{Pt}}=2.77$ Å and $a_{\text{FeO}}=3.04$ Å, respectively) results in a complex misfit moiré structures for 1- and 2-monolayer (ML) FeO films.^{16,17,18,19,20,21} Roughly speaking, the positions of the iron and oxygen atoms in these structures are modulated between the fcc and hcp sites with a periodicity corresponding to the misfit parameter.^{16,20} The experimentally determined incommensurate moiré structure has a periodicity of approximately (9x9) with respect to the Pt(111) substrate, additionally indicating a rotational mismatch on the order of several degrees.^{16,18} While an unsupported FeO(111) monolayer is perfectly flat, the interaction and charge exchange with the Pt(111) substrate induce a separation of iron and oxygen atomic planes²² of the order of 0.7 Å, considerable smaller compared with 1.24 Å in bulk FeO.¹⁷

Beyond a thickness of 2 ML, the preferential formation of magnetite (Fe_3O_4) is observed.²³ However, it was shown recently that the FeO(111) films on Pt(111) can be stabilized to a thickness of several nanometers using a carefully adapted preparation.¹³ These films display electronic and magnetic properties markedly different from wüstite. Specifically, the hyperfine interactions probed by conversion electron Mössbauer spectroscopy (CEMS) indicate a high degree of covalency in the Fe-O bonds and long-range magnetic order in the thickness range of a few monolayers. It has been suggested that these unusual properties signify a new metastable crystalline phase that is stabilized by epitaxial growth. The present study of vibrational properties using the nuclear resonance scattering (NRS) of synchrotron radiation combined with the *ab initio* phonon calculations sheds light on this question.

Experiments were performed in a multi-chamber ultrahigh vacuum system²⁴ at the NRS ID18-beamline²⁵ in ESRF Grenoble. ⁵⁷FeO films with a thickness d in a range from 1 to 16 ML (1 ML is equivalent to 2.48 Å of bulk FeO) were epitaxially grown on an atomically clean Pt(111) substrate using the preparation protocol described earlier,¹³ and the sample structure was verified *in situ* using characteristic LEED patterns as a function of the thickness. Prior to the NIS experiments the samples were characterized by the coherent grazing-incidence NRS measurements²⁶. The \vec{k} vector of the incident X-rays was parallel (within $\pm 3^\circ$) to the dense-packed direction on the Pt(111) surface. The NRS time spectra shown in Fig.1 together with the best fits using the REFTIM software²⁷ (solid lines) coincide with the previous CEMS measurements for another set of samples.¹³ The quantum beat modulation of the scattered intensity decay that appears at approximately 6 ML reveals long-range magnetic order with the average hyperfine magnetic field B_{hf} increasing from $(23.1 \pm 0.2)\text{T}$ at 6 ML to $(28 \pm 1)\text{T}$ at 10 ML. Above this thickness B_{hf} dropped to almost zero within few monolayers when the high- and low- B_{hf} phases coexisted. For the high- B_{hf} phase, the numerical analysis of the time spectra explicitly indicated the ferromagnetic order with the magnetization along a unique direction, namely at $(30 \pm 5)^\circ$ with respect to \vec{k} . It is not clear whether the magnetic transition above 10 ML is to the paramagnetic or to the antiferromagnetic state with a low magnetic moment.

The unusual electronic and magnetic properties of the FeO layers are accompanied by atypical features of the NIS spectra (see Supplementary Material at [...]), which measure the probability of the phonon-assisted nuclear resonance absorption of synchrotron radiation as a function of the detuning energy ΔE from the 14.412 eV resonance for ⁵⁷Fe. The NIS spectra in Fig.2(bottom) show clear changes with the FeO thickness. The most characteristic is the strong intensity enhancement at low energies for the thinnest films (1ML and 2ML), and the sharp peak at approximately 25 meV, which got smeared in the thickness range where the magnetic order persists.

The partial iron PDOS, $g(E)$, can be derived from the NIS spectra in a parameter-free procedure, which considers the thermal population of phonons and multi-phonon processes.^{28,29} Due to the grazing incidence geometry, PDOS corresponds to phonons with a large in-plane component of the polarization vector along the direction given by the projection of the X-ray \vec{k} -vector on the sample surface. The PDOS presented in Fig.2 are distinctly

different from that of bulk wüstite,^{30,31} which is characterized by a broad peak at 20 meV and an even broader tail centered at 30 meV and extending to approximately 40 meV. The most characteristic features of PDOS in Fig. 2 are: (i) a sharp peak at 23.5 meV and a sudden cutoff for the thinnest and thickest films, (ii) a clear correlation between the smearing of PDOS and the magnetic order for intermediate thicknesses (6 – 10 ML), (iii) phonon hardening above the thickness of the magnetic anomaly, and (iv) a deviation from the 3D $\propto E^2$ Debye behavior revealed in the low energy range for the 1 and 2 ML films. The power n in the $g(E) \propto E^n$ dependence at low E within the Debye approximation relates to the system dimensionality D : $n=D-1$, and hence, $n=2$ is common for 3-dimensional systems, while $n=1$ corresponds to 2-dimensional behavior. The linear $g(E)$ dependence for low-dimensional systems is the subject of a long debate due to controversies between experiments (NIS or neutron scattering) on different nanoparticle assemblies, for which linear,^{32,33,34} quadratic^{35,36,37,38} and fractional^{39,40,41} energy dependencies have been reported. This diverse behavior reflects the complexity of nanomaterials, for which the reduced dimensionality of the surface atoms overlaps with the different local coordination and finite size effects, as discussed theoretically.^{42,43} For a model 2D interfacial system was observed, i.e. for the Fe monolayer on W(110),⁴⁴ PDOS, albeit very different in the overall character from bulk Fe, displayed typical $\propto E^2$ Debye behavior in the long wavelength limit. Reasonably, the prerequisite for the 2-dimensional character of the surface phonons is a kind of decoupling between the surface and the interior, as shown by Sun et al.,³⁴ which is not realized for neither the metallic isostructural systems⁴⁴ nor the surface of a metal single crystal.⁴⁵

In contrast, the two-dimensional behavior is demonstrated clearly for our epitaxial FeO films on Pt(111) in the ultrathin limit in Fig.3(top), where the low energy experimental points of $g(E)$ are shown in the double logarithmic plot. In such a plot, the slope of the linear fits represents the power n in the $g(E) \propto E^n$ dependence. The fitted $n=1.0 \pm 0.05$ precisely points to the 2D Debye solid for 1 and 2 ML within the limit of the experimental error. The power n increases to $n=1.5 \pm 0.06$ for $d=4$ ML and nearly reaches the 3D limit for $d \geq 9$ ML, with an average of $\langle n \rangle = 1.94 \pm 0.05$. The thickness evolution of the power n that scales with the reciprocal of the film thickness suggests that the FeO films with the vibrational characteristic which is independent of the Pt(111) substrate can be treated as quasi free-standing. Remarkably, from the point of view of the continuous medium Debye model, the truly 2D system is not only the monolayer but also the bilayer FeO film.

The 2-dimensional characteristic of PDOS for the monolayer FeO films on Pt(111) and the strong deviation from the vibrational bulk-FeO characteristics are related to the special structure of the FeO films, as studied in detail in the monolayer limit both experimentally^{16,17,18,46} and theoretically.^{20,21} A large misfit between the Pt(111) and FeO(111) planes leads to the moiré structure that has been explained by the modulation of the local interaction with the substrate, depending on the position of the iron and oxygen atoms with respect to the platinum substrate. According to Giordano et al.,²⁰ the strongest FeO-Pt interaction occurs when both the Fe and O atoms are located within the hollow Pt(111) sites (“Fe-fcc”) and the weakest when the Fe atom is located in the on-top position with respect to a surface Pt atom. For the latter case, the structural properties of the FeO/Pt(111) monolayer are similar to those of a free-standing FeO monolayer,²⁰ which can account for the 2-dimensional vibrational characteristics.

We compared the PDOS results with the first principle calculations to elucidate the observed features. The model was built using five fcc-Pt layers (80 atoms) stacked along the (111)-direction and covered on one side by an FeO monolayer (32 atoms) and a 1.8-nm thick vacuum layer. This structure was optimized using the projector-augmented wave method⁴⁷ and the generalized-gradient approximation within the VASP program.⁴⁸ Iron oxide was treated with the DFT+U approach ($U_{\text{Fe}}-J_{\text{Fe}} = 3$ eV) which has been shown to satisfactorily reproduce the essential structural and energetic characteristics of thin, Pt-supported FeO_x films.⁴⁹ The volume of the supercell was held constant, while atomic positions were fully relaxed. We assumed an antiferromagnetic order for the Fe atoms, which provides lower energy than the ferromagnetic and nonmagnetic states.²⁰ The dipole correction perpendicular to the surface was added to the potential to improve the convergence of the total energy.

The phonon spectra were calculated using the direct method implemented in the Phonon software.⁵⁰ The force constants and dynamical matrices were derived by displacing all non-equivalent atoms from equilibrium positions and calculating the Hellmann-Feynman forces. The PDOS was obtained by randomly sampling the k-points in the first Brillouin zone.

We adopted a strategy proposed by Giordano et al.²⁰ for the theoretical description of the FeO monolayer to account for the large unit cell of the actual FeO/Pt(111) interface. Three different pseudomorphic configurations corresponding to the different regions of the moiré

unit cell were considered as a starting point for structure optimization. The only stable pseudomorphic structure as a result of optimization was “Fe-fcc” (both O and Fe ions in three-fold hollow sites of a Pt(111) substrate). In the course of optimization, the “Fe-hcp” (O ions on-top of surface Pt atoms, Fe ions in the hollow sites) structure relaxed to “Fe-fcc,” and the “Fe-top” (O ions in the hollow sites, Fe ions on-top of a surface Pt) structure relaxed to a new structure in which Fe atoms occupied intermediate positions. It can be concluded that only the fcc regions stabilize the moiré structures and we will focus on the phonon spectra obtained for this region in the following.)

The calculated partial Fe PDOS functions for the “Fe-fcc” structure decomposed in the X, Y (in-plane) and Z (normal) directions are shown in Fig. 4. The vibrational characteristic is strongly anisotropic, and the Y component is compared with the experimental results in Fig.4b because the \vec{k} vector of the X-rays in the NIS experiment was nearly parallel to the Y-direction. Despite the simplifications in the theoretical model, the agreement between the experiment and theory is extremely good. This means that the internal structure of the FeO layer rather than its interaction with the substrate determines the vibrational properties. Additionally, the calculations reveal high energy vibration of the Fe atoms above 47 meV that were not observed in the bulk rock-salt structure.³¹

While the explanation of the vibrational properties of the thicker FeO layers is less straightforward because their increased structural complexity is a severe limitation to theoretical modeling, notwithstanding the anomaly in PDOS, which accompanies the long-range magnetic order, as it is discussed below, the main features of PDOS are similar over the thickness range from 1 to 16 ML. The most characteristic features: the peak at approximately 25 meV and the sharp cutoff above this energy are preserved for the thickest (4-nm) FeO film, with only a slight phonon stiffening as compared to the monolayer limit. Such a blue shift can be generally expected as a result of the enhanced system stiffness, however, it was recently shown that the detail balance of different factors contributing to the force constants in oxide systems is complex.⁵¹ Nevertheless, the distinct dissimilarity to the phonon spectra of bulk wüstite³⁰ or an epitaxial magnetite film⁵² clearly indicate a new artificial FeO structure that was stabilized on Pt(111).

Finally, we discuss the magnetic anomaly reflected in the phonon spectra for 6 to 10 ML. A magnetic transition, also if not accompanied by a structural one, can substantially modify the

vibrational properties in the bulk, by changing all phonon characteristics, such as frequency, intensity and spectral line width.⁵³ The long range magnetic order may be also responsible for the stabilization of the crystal structure,⁵⁴ which is of particular importance for epitaxial metastable systems.⁵⁵ For metallic ultrathin fcc-Fe(001) films on Cu(1001) Benedek et.al.⁵⁶ showed a pronounced temperature dependence of the phonon frequency with a sharp increase below the Curie temperature for a given constant thickness of 6 ML. For Fe(110) films on W(110) the influence of the ferromagnetic order that emerged with the increasing film thickness on the phonon spectra was masked by strong structural effects, i.e. the loss of pseudomorphicity between 1 and 2 ML. For the present case of the FeO films, a model situation takes place, when the magnetic order is established with only minor structural changes, as judged from the LEED pattern. Hence, the broadening in the phonon spectra for 6 to 10 ML we interpret as the effect of the spin ordering, which may result in magnetostrictive strains and a lattice distortion. When the ferromagnetic order vanishes above 10 ML, the PDOS sharpens again, however the main peak remains by a factor of two broader than the exceptionally narrow peak for 1 ML that has the full width at half maximum approaching the experimental resolution of 2 meV. Similar situation was observed for MnO(100) films on Pt(111), when the monolayer showed very narrow phonon features compared to thicker films.⁵⁷ The thickness dependent PDOS broadening results from the increased structural complexity of the thicker FeO films due to lacking translational symmetry along the film normal and a possible modulation of the interplanar distances. The detailed determination of the unusual thick-FeO film structure is the subject of the ongoing research.

Acknowledgments

This work was supported by the National Science Center Poland (NCN) under Project No. 2011/02/A/ST3/00150). PP acknowledges support by NCN under Project No. 2012/04/A/ST3/00331. The research was performed in the framework of the Marian Smoluchowski Krakow Research Consortium- Leading National Research Centre (KNOW), which is supported by the Ministry of Science and Higher Education of Poland.

¹ A. C. Ferrari, J.C. Meyer, V. Scardaci, C. Casiraghi, M. Lazzeri, F. Mauri, S. Piscanec, D. Jiang, K.S. Novoselov, S. Roth, and a. K. Geim, *Phys. Rev. Lett.* **97**, 1 (2006).

² P. Miró, M. Audiffred, and T. Heine, *Chem. Soc. Rev.* **43**, 6537 (2014).

³ P. Piekarczyk, K. Parlinski, and A.M. Oleś, *Phys. Rev. Lett.* **97**, 156402 (2006).

⁴ *Oxide Ultrathin Films: Science and Technology*, G. Pacchioni, Sergio Valeri (Editors), Wiley 2012

-
- ⁵ A. Rohrbach, J. Hafner, and G. Kresse Phys. Rev. B **70**, 125426 (2004).
- ⁶ Y. Li, K. Yao, Z. Liu, and G. Gao, Phys. Rev. B **72**, 155446 (2005).
- ⁷ G. Kresse, M. Schmid, E. Napetschnig, M. Shishkin, L. Köhler, and V. Peter, Science **308**, 1440 (2005).
- ⁸ D. Wu, M.G. Lagally, and F. Liu, Phys. Rev. Lett. **107**, 2 (2011).
- ⁹ C. Tusche, H.L. Meyerheim, and J. Kirschner, Phys. Rev. Lett. **99**, 2 (2007).
- ¹⁰ S. Schumacher, D.F. Förster, F. Hu, T. Frauenheim, T.O. Wehling, and T. Michely, Phys. Rev. B **89**, 1 (2014).
- ¹¹ J. Goniakowski, C. Noguera, and L. Giordano, Phys. Rev. Lett. **93**, 215702 (2004)
- ¹² W. Weiss and W. Ranke, Prog. Surf. Sci. **70**, 1 (2002).
- ¹³ N. Spiridis, D. Wilgocka-Ślęzak, K. Freindl, B. Figarska, T. Giel, E. Młyńczak, B. Strzelczyk, M. Zając, and J. Korecki, Phys. Rev. B **85**, 075436 (2012).
- ¹⁴ W. Sturhahn, T. Toellner, E. Alp, X. Zhang, M. Ando, Y. Yoda, S. Kikuta, S. M, C. Kimball, and B. Dabrowski, Phys. Rev. B **74**, 3832 (1995).
- ¹⁵ M. Seto, Y. Yoda, S. Kikuta, X. Zhang, and M. Ando, Phys. Rev. Lett. **74**, 3828 (1995).
- ¹⁶ H. Galloway, P. Sautet, and M. Salmeron, Phys. Rev. B **54**, R11145 (1996).
- ¹⁷ Y.J. Kim, C. Westphal, R.X. Ynzunza, H.C. Galloway, M. Salmeron, M. a. Van Hove, and C.S. Fadley, Phys. Rev. B **55**, R13448 (1997).
- ¹⁸ M. Ritter, W. Ranke, and W. Weiss, Phys. Rev. B **57**, 7240 (1998).
- ¹⁹ W. Ranke, M. Ritter, and W. Weiss, Phys. Rev. B **60**, 1527 (1999).
- ²⁰ L. Giordano, G. Pacchioni, J. Goniakowski, N. Nilius, E. Rienks, and H.-J. Freund, Phys. Rev. B **76**, 075416 (2007).
- ²¹ W. Zhang, Z. Li, Y. Luo, and J. Yang, J. Phys. Chem. C **113**, 8302 (2009).
- ²² J. Goniakowski, C. Noguera, L. Giordano, G. Pacchioni, Phys. Rev. B **80** 125403 (2009)
- ²³ W. Weiss and M. Ritter, Phys. Rev. B **59**, 5201 (1999).
- ²⁴ S. Stankov, R. Rüffer, M. Sladeczek, M. Rennhofer, B. Sepiol, G. Vogl, N. Spiridis, T. Slezak, and J. Korecki, Rev. Sci. Instrum. **79**, 045108 (2008).
- ²⁵ R. Rüffer and A.I. Chumakov, Hyperfine Interaction, **97/98** (1996) 589-604.
- ²⁶ Grazing time spectra
- ²⁷ M. Andreeva, B. Lindgren, V Panchuk, REFTIM, Version 7.4,
www.esrf.eu/computing/scientific/REFTIM/MAIN.htm
- ²⁸ A.I. Chumakov, W. Sturhahn, Hyperfine Interactions **123/124**, 781 (1999)
- ²⁹ V.G. Kohn, A.I. Chumakov, Hyperfine Interactions **125**, 205 (2000)
- ³⁰ V. Struzhkin, H. Mao, J. Hu, M. Schwoerer-Böhning, J. Shu, R. Hemley, W. Sturhahn, M. Hu, E. Alp, P. Eng, and G. Shen, Phys. Rev. Lett. **87**, 255501 (2001).
- ³¹ U. Wdowik, P. Piekarz, K. Parlinski, A. M. Oleś, and J. Korecki, Phys. Rev. B **87**, 121106 (2013).

-
- ³² U. Stuhr, H. Wipf, K. Andersen, and H. Hahn, Phys. Rev. Lett. **81**, 1449 (1998).
- ³³ A. Kara and T. Rahman, Phys. Rev. Lett. **81**, 1453 (1998).
- ³⁴ D. Sun, X. Gong, and X.-Q. Wang, Phys. Rev. B **63**, 193412 (2001).
- ³⁵ B. Fultz, C. C. Ahn, E. E. Alp, W. Sturhahn, and T. S. Toellner, Phys. Rev. Lett. **79**, 937 (1997).
- ³⁶ H.N. Frase, B. Fultz, and J. L. Robertson, Phys. Rev. B **57**, 898 (1998).
- ³⁷ Pasquini, A. Barla, A. I. Chumakov, O. Leupold, R. Rüffer, A. Deriu, and E. Bonetti, Phys. Rev. B **66**, 073410 (2002)
- ³⁸ B. Papandrew, A. F. Yue, B. Fultz, I. Halevy, W. Sturhahn, T.S. Toellner, E. E. Alp, and H. Mao, Phys. Rev. B **69**, 144301 (2004).
- ³⁹ Hu, G. Wang, W. Wu, P. Jiang, and J. Zi, J. Phys.: Condens. Matter **13**, L835 (2001).
- ⁴⁰ M. Derlet, R. Meyer, L. J. Lewis, U. Stuhr, and H. Van Swygenhoven, Phys. Rev. Lett. **87**, 205501 (2001).
- ⁴¹ B. Roldan Cuenya, L.K. Ono, J.R. Croy, K. Paredis, A. Kara, H. Heinrich, J. Zhao, E.E. Alp, A.T. DelaRiva, A. Datye, E.A. Stach, and W. Keune, Phys. Rev. B **86**, 165406 (2012).
- ⁴² A. Kara, T.S. Rahman / Surface Science Reports **56**, 159 (2005).
- ⁴³ C. Hudon, R. Meyer, and L. Lewis, Phys. Rev. B **76**, 045409 (2007).
- ⁴⁴ S. Stankov, R. Röhlberger, T. Ślęzak, M. Sladeczek, B. Sepiol, G. Vogl, A. I. Chumakov, R. Rüffer, N. Spiridis, J. Łażewski, K. Parliński, and J. Korecki, Phys. Rev. Lett. **99**, 185501 (2007).
- ⁴⁵ T. Ślęzak, J. Łażewski, S. Stankov, K. Parlinski, R. Reitering, M. Rennhofer, R. Rüffer, B. Sepiol, M. Ślęzak, N. Spiridis, M. Zając, A. I. Chumakov, and J. Korecki, Phys. Rev. Lett. **99**, 066103 (2007).
- ⁴⁶ G. H. Vurens, M. Salmeron, and G. A. Somorjai, Surf. Sci. **201**, 129 (1988)
- ⁴⁷ P. E. Blochl, Phys. Rev. B **50**, 17953 (1994).
- ⁴⁸ G. Kresse and J. Furthmüller, Comput. Mater. Sci. **6**, 15 (1996).
- ⁴⁹ S. Prada, L. Giordano, G. Pacchioni, C. Noguera, Goniakowski, J. Chem. Phys. **141**, 144702-9 (2014)
- ⁵⁰ Parlinski, Z. Q. Li, and Y. Kawazoe, Phys. Rev. Lett. **78**, 4063 (1997); K. Parlinski, Software Phonon, Cracow, 2012.
- ⁵¹ C. Bhandari and W.R.L. Lambrecht, Phys. Rev. B **89**, 1 (2014).
- ⁵² B. Handke, A. Kozłowski, K. Parliński, J. Przewoźnik, T. Ślęzak, A. I. Chumakov, L. Niesen, Z. Kąkol, and J. Korecki, Phys. Rev. B **71**, 144301 (2005).
- ⁵³ R. Haumont, J. Kreisel, P. Bouvier, and F. Hippert, Phys. Rev. B **73**, 2 (2006)
- ⁵⁴ K. Parlinski and J. Łażewski, Europhys. Lett. **56**, 275 (2001)
- ⁵⁵ J. Łażewski, P. Piekarczyk, A.M. Oleś, J. Korecki, and K. Parlinski, **76**, 205427 (2007).
- ⁵⁶ G. Benedek, E. Hulpke, and W. Steinhögl, Phys. Rev. Lett. **87**, 027201 (2001).
- ⁵⁷ S. Sachert, S. Polzin, K. Kostov, and W. Widdra, Phys. Rev. B **81**, 195424 (2010).

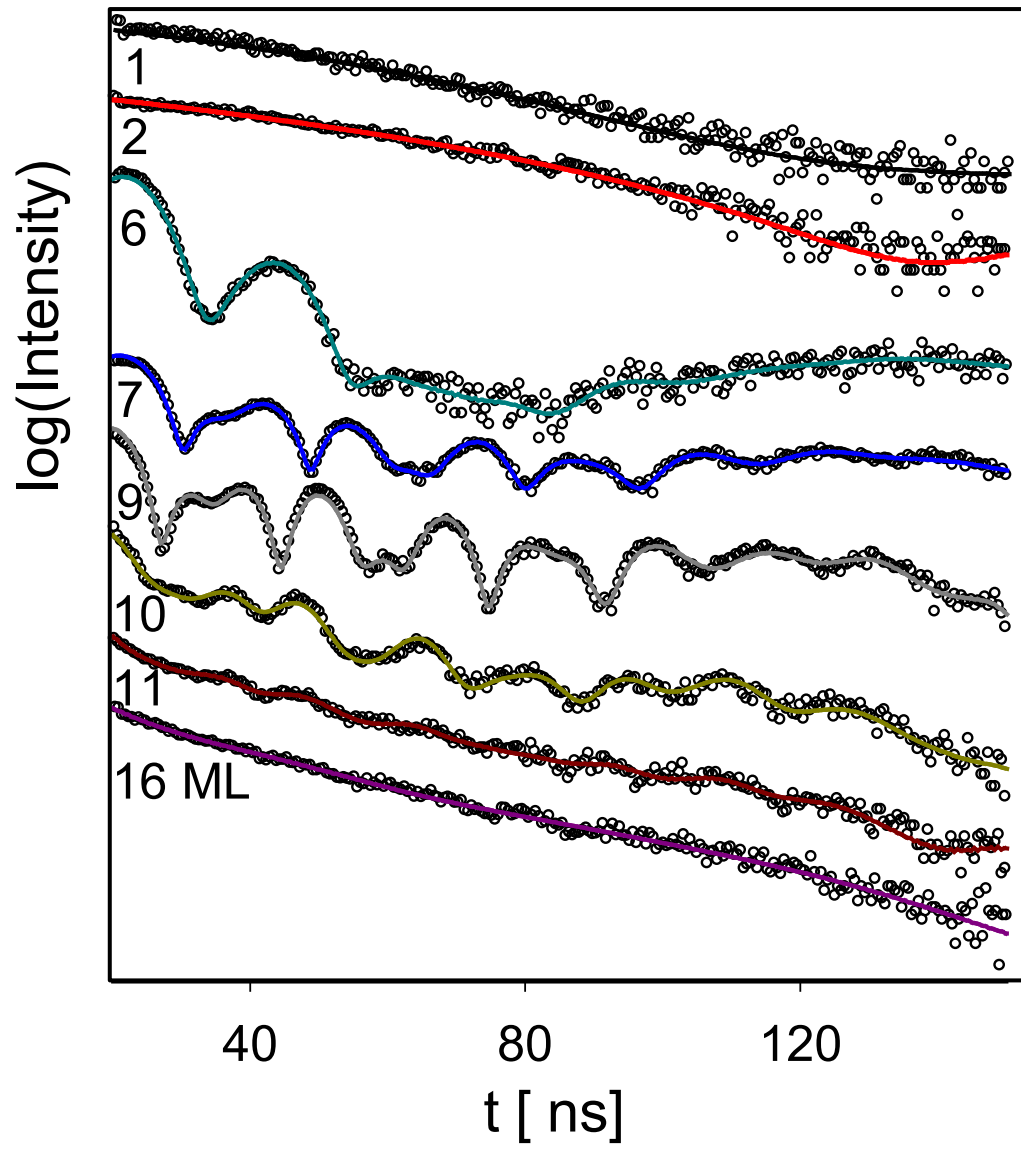


Fig.1. NRS time spectra for $^{57}\text{FeO}/\text{Pt}(111)$ as a function of FeO film thickness given in monolayers.

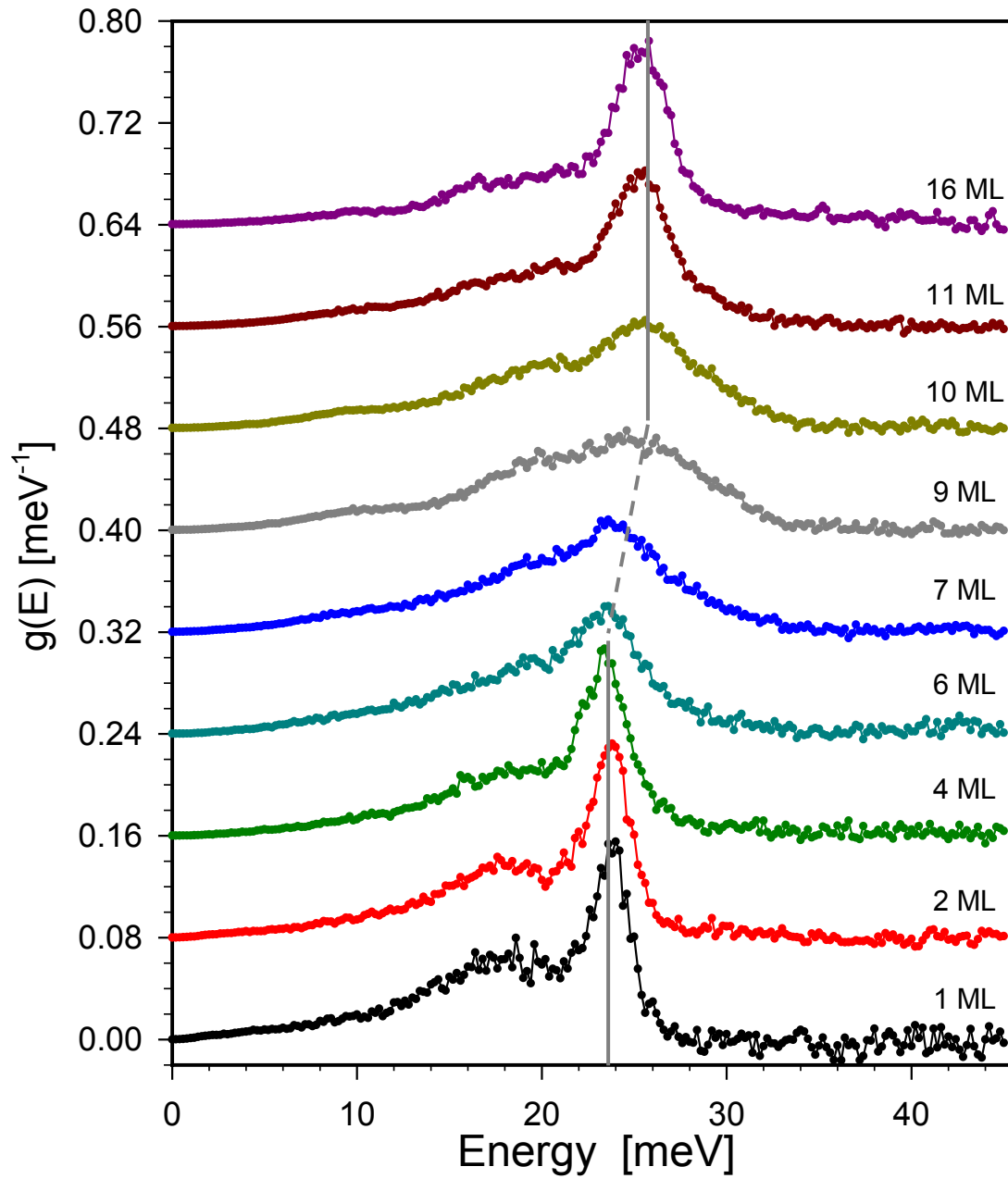


Fig.2. Phonon DOS $g(E)$ for FeO(111) films on Pt(111) as a function of thickness. For clarity, the plots are vertically shifted by 0.08 meV^{-1} . The vertical lines mark the shift of the high energy phonon peak.

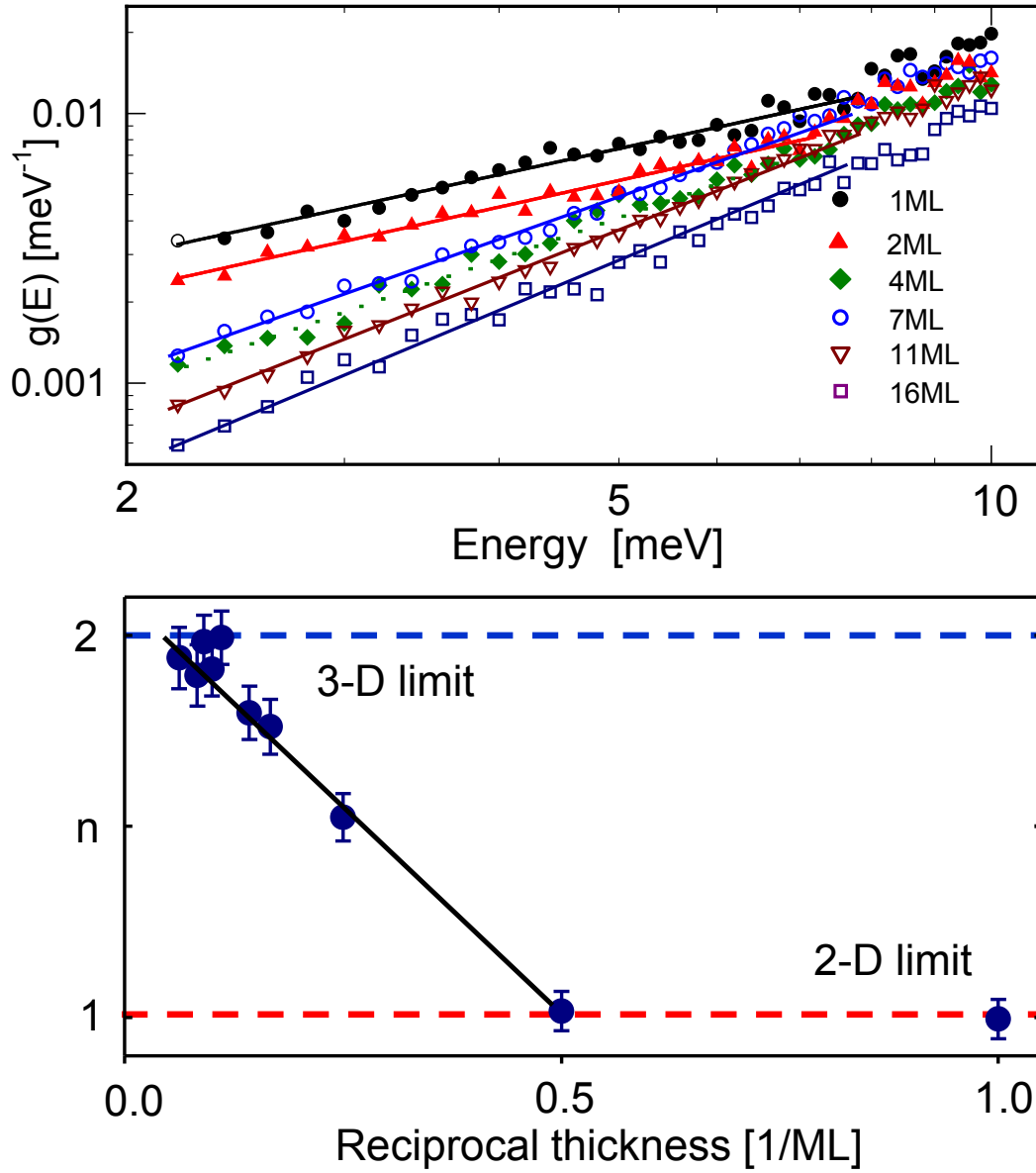


Fig.3. (Top) Double logarithmic plot of the phonon density of state $g(E)$ for low energy. The straight lines are the fits of the experimental points to a power $g(E) \propto E^n$ dependence. (Bottom) The plot of the power n as a function of the reciprocal of the FeO film thickness d (in ML). The horizontal lines at $n=1$ and $n=2$ are the 2D and 3D limits, respectively.

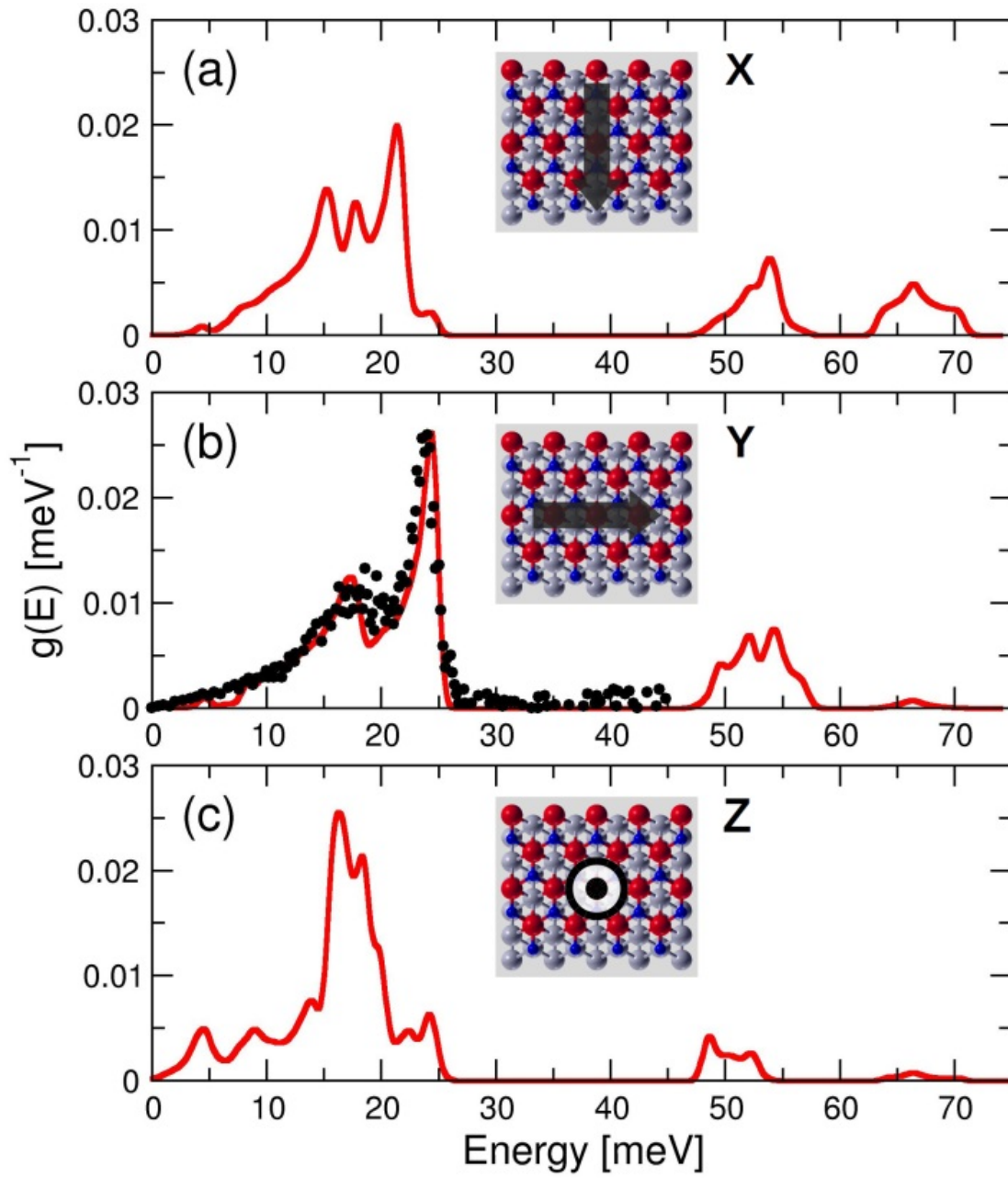


Fig.4. Partial Fe PDOS for the “Fe-fcc” structure of the FeO monolayer decomposed in the X, Y and Z directions. Insets depict the X-Y-Z orientation on a top view of the stick and ball model of the 1 ML FeO/Pt(111) system (Pt atoms are light gray, Fe atoms are red/large dark gray, O atoms are blue/small dark gray).

Supplementary Material

An example of the measured spectra for the thickest 16 ML FeO film is shown in Fig. 1 (top) on a logarithmic scale (black curve) to visualize the elastic peak, which is more intense by two orders of magnitude than the phonon-assisted events. The elastic peak must be subtracted for further analysis, as shown in Fig. 2 (bottom), where error bars have been added to the experimental points. Large error values near $\Delta E=0$ are the result of the elastic peak subtraction, and the elastic peak range, i.e., the energy range of approximately ± 2 meV, corresponding to the instrumental energy resolution, should be excluded from the analysis. The NIS spectra in Fig. 2 (bottom) show clear changes with the FeO thickness. The most characteristic is the strong intensity enhancement at low energies for the thinnest films (1 ML and 2 ML), and the sharp peak at approximately 25 meV, which got smeared in the thickness range where the magnetic order is observed.

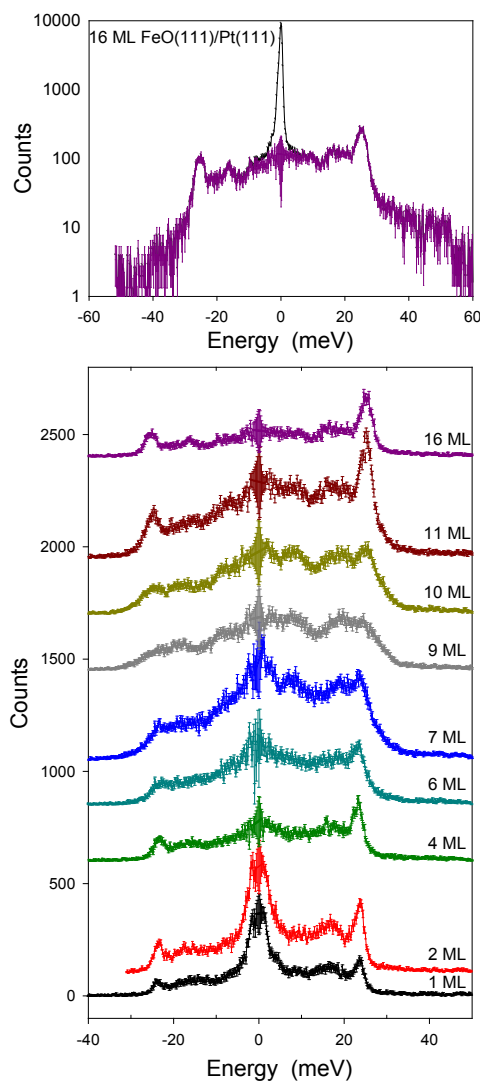


Fig. 1. (Top) The NIS spectrum for the 16 ML FeO film (black/continuous line), shown on a logarithmic scale to visualize the elastic peak. The error bars represent the statistical errors and the errors due to the uncertainty of the elastic peak subtraction procedure. (Bottom) NIS spectra after subtraction of the elastic peak as a function of the FeO film thickness. The spectra are vertically offset for clarity.